Journal of Power Sources Advances 26 (2024) 100140

Contents lists available at ScienceDirect

Journal of Power Sources Advances

journal homepage: www.sciencedirect.com/journal/journal-of-power-sources-advances

In situ polymerized poly(1,3-dioxolane) in polyacrylonitrile porous scaffolds: A novel composite polymer electrolyte for room temperature battery application

Nicolò Albanelli [a], Francesco Capodarca [a], Michele Zanoni [a], Giampaolo Lacarbonara [a], Maria Letizia Focarete [a,b], Chiara Gualandi [a,b,c], Catia Arbizzani [a,*]

[a] Department of Chemistry "Giacomo Ciamician", Alma Mater Studiorum - University of Bologna, Via F. Selmi 2, 40126, Bologna, Italy
[b] Health Sciences & Technologies Interdepartmental Center for Industrial Research, Alma Mater Studiorum - University of Bologna, Via Tolara di Sopra 41/E, Ozzano Emilia, 4006, Bologna, Italy
[c] Interdepartmental Center for Industrial Research on Advanced Applications in Mechanical Engineering and Materials Technology, Alma Mater Studiorum - University of Bologna, Viale Risorgimento, 2, 40136, Bologna, Italy

ARTICLE INFO

Keywords:
Electro-initiated polymerization
Electrospun membrane
PAN
PDOL
poly(1,3 dioxolane)
Polymer electrolyte

ABSTRACT

The need for high-energy and safe batteries is more and more urgent, and a possible approach is to use solid polymer electrolyte with high conductivity combined with lithium metal anode. Poly (1,3-dioxolane)-based electrolytes are promising, and the feasibility to polymerize 1,3-dioxolane (DOL) in situ makes this approach very attractive. In this paper, we present the in situ electro-initiated polymerization of DOL in polyacrylonitrile nanofibrous mats, without using initiator or crosslinking agents. The amount of monomer loaded in the porous scaffold, the electrochemical technique used to initiate the polymerization and the salt amount were investigated as important parameters that affect the ion conductivity and the performance of the obtained polymer electrolyte. Particular attention was directed towards minimizing the presence of residual monomer in the resulting polymer, with the aim of progressing towards the development of a real solid-state polymer electrolyte. The results of the thermal, morphological, and electrochemical characterization are reported and discussed.

1. Introduction

Batteries are crucial for a wide range of applications, and at present, the most exploited chemistry is based on lithium ions, in which the electrolyte usually consists of lithium salt and carbonate-based organic solvent. The toxicity, the narrow working temperature, the decomposition under high voltage and the low ignition point of the electrolytic medium are the main safety concerns of this technology [1]. In addition, the conventional separators soaked with the liquid electrolytes do not assure the suppression of lithium dendrite growth in the high-energy battery of the future based on lithium metal anode. For this reason, advances in material chemistry have been reached by the solid-state chemists' creativity and innovation in the design and elaboration of new solid electrolytes [2]. Polymer electrolytes are safer than liquid ones as they do not give leakage problems and because of their non-toxicity, low vapor pressure, and non-flammability. The majority of dry solid polymer electrolytes reported so far and based on high molecular weight poly (ethylene oxide) (PEO) with different Li^+ salts, suffers from poor conductivity at room temperature [3]. The Li^+ conduction, occurring via the complexation of the ions with the O atoms in the chain that permits the ionic motion, strongly depends on the degree of crystallinity of the polymer. For making the polymer more amorphous and, in turn, for improving the ionic conductivity, big anions, plasticizers and even low amounts of solvents or ionic liquids have been added to the polymer electrolytes [4]. As an example, for the Gen 4 Li metal batteries, the strategy of using inorganic solid electrolyte has been pursued. However, the interface contact between the electrodes and the electrolyte is still an issue, and composite polymer/ceramic electrolytes have been proposed to mitigate it [5].

Recently, great attention has been focused on (1,3-dioxolane) (DOL) and on its possibility to be easily polymerized to give poly (1,3-dioxolane) (PDOL), as the group of D. Aurbach demonstrated more than 30 years ago [6,7]. PDOL has been already proposed as a protective layer in Li/S cells [8–10], as an artificial solid electrolyte interphase (SEI) for

* Corresponding author.
E-mail address: catia.arbizzani@unibo.it (C. Arbizzani).

https://doi.org/10.1016/j.powera.2024.100140
Received 31 October 2023; Received in revised form 15 January 2024; Accepted 2 February 2024
Available online 9 February 2024

lithium metal anode [11] and for the first time it was proposed also by the group of C. Arbizzani [10] as a protective layer for high-voltage cathodes, such as LNMO, on which DOL was polymerized electrochemically. In Li/S cells, PDOL does not only inhibit the polysulfides diffusion but also protects the Li metal anode as quasi-solid electrolyte [8]. The obtained solid electrolyte resulted to be mechanically flexible, showing also self-sealing and seal-healing properties [9]. A pioneering work was also carried out in 2007 by L. Kong et al. [12] on the fabrication of a Li/$LiCoO_2$ battery with a DOL-based electrolyte by accurately controlling the DOL electropolymerization through adjustment of the applied current rate. The renewed interest in utilizing PDOL as an electrolyte stems from its elevated oxygen atom content (43.2 wt%), which surpasses that of PEO (36.4 wt%). This higher oxygen content suggests an increased number of interaction sites for cations when compared to PEO-based electrolytes. This can facilitate the ion transport through the polymer backbones which could lead to a higher ionic conductivity [13]. Wang et al. demonstrated that the binding energy between lithium ion and O in PEO was −1.725 eV, while in PDOL the binding energy is −1.225 eV per bond, given that lithium ion coordinates with two adjacent oxygen atoms. This relatively weaker interaction is beneficial for Li ion transport [13]. In the last few years plenty of papers have been published on DOL polymerization for achieving a suitable solid or quasi solid polymer electrolyte. Most of these papers deal with electropolymerization in presence of initiators [14–17], which could be salts or inorganic particles like those of NASICON-type lithium ionic conductors [18–21] and/or those of a crosslinker [22,23], sometimes also in presence of a supporting membrane because of its poor mechanical properties [13,17,24,25].

In the present paper we added a LiTFSI-DOL solution to a dry electrospun poly (acrylonitrile) (PAN) scaffold. PAN has been previously used as polymer hosts in solid and gel polymer electrolytes [26–28]. Indeed, its nitrile groups can coordinate and solvate Li ions, its high oxidation potential makes viable the polymerization of DOL without affecting PAN skeleton and it has a good electrolyte uptake. On the contrary, the stability of PAN in solid or gel electrolytes in contact with Li metal is still an open question [26]. The nitrile groups can help the growth of a LiF-rich SEI layer in presence of fluoroethylene carbonate due to the strong interaction of the two dipoles [29]. The strategy of polymer-in-salt electrolyte has also been pursued to form a stable Li/electrolyte interphase in presence of PAN-LiTFSI [30]. We did not use any initiator or crosslinker for DOL polymerization, which gave us the possibility to wet the electrode before starting the polymerization and to control the polymerization by changing the electrochemical technique or the composition of the solution. Different electrochemical techniques have been used to electro-initiate the in situ polymerization of the DOL, and the electrolyte volume and concentration have been investigated in order to elucidate the effect of the possible residues of liquid DOL in the system after polymerization. The proposed approach aims at minimizing the presence of a liquid phase and move towards a real solid state polymer electrolyte. The obtained polymer has been characterized by thermal and mechanical analyses, by morphology and spectroscopic investigation. Electrochemical characterization has also been carried out by impedance spectroscopy measurements and by the conventional electrochemical techniques.

2. Experimental section

2.1. Materials

Lithium bis(trifluoromethanesulfonyl)imide (LiTFSI, Sigma-Aldrich, Merck Life Science S.r.l., Milan, Italy) was dissolved in 1,3-dioxolane (DOL, Sigma-Aldrich, Merck Life Science S.r.l., Milan, Italy) to obtain two solutions with different salt concentrations: one with a LiTFSI concentration of 1.7 molal and an O:Li ratio of 16:1 and the other one with a concentration of 5 molal, resulting in an O:Li ratio of ca. 5:1.

2.2. Electrospun scaffold preparation

A polyacrylonitrile (PAN, $M_w = 150000$ g mol^{-1}, Merck Life Science S.r.l., Milan, Italy) mat prepared by electrospinning was used as the scaffold for the electrolyte. The electrospun mat was fabricated using an in-house electrospinning apparatus consisting of a high-voltage power supply (Spellman SL b50 P 10/CE/230), a syringe pump (KD Scientific 200 series) and a glass syringe filled with the polymer solution. The syringe was connected to a blunt, stainless-steel needle (inner diameter = 0.51 mm) through a polytetrafluoroethylene (PTFE) tube. Fibers were collected on an aluminum rotating collector (length = 120 mm, diameter = 60 mm) with a rotation speed of 100 rpm. Electrospinning was carried out at room temperature with a relative humidity of 40–50%. The polymer was dissolved in DMF at a concentration of 9% w/v. The polymer solution was electrospun using an applied voltage of 20.5 kV, a feed rate of 1.0 mL h^{-1}, and a needle-to-collector distance of 20 cm.

2.3. PDOL polymerization

The obtained electrospun mat was dried and disks of 10 mm in diameter were cut and impregnated with a certain amount of LiTFSI-DOL solution. T-shaped BOLA cells (BOLA, Bohlender GmbH, Grünsfeld, Germany) were assembled inside an Argon filled dry box (Labmaster 130, H_2O and $O_2 < 0.1$ ppm, MBraun, Germany) for the in situ electro-initiated polymerization of DOL and to perform the electrochemical characterization by using a Biologic VSP potentiostat/galvanostat. The selection of the electrochemical technique for the electro-initiated polymerization of DOL was carried out by using Li//stainless steel (SS) cell (Li, Sigma Aldrich, 0.75 mm thick, 99.9%).

2.4. Characterization methods

The electrolyte uptake of the PAN mat was determined in triplicate by soaking the PAN disks (10 mm in diameter) in 1.7 *m* LiTFSI-DOL solution. The disks were dipped in the solution for 24 h and then the liquid excess was gently wiped off. The weight of the imbibed PAN was compared to the one of the dry PAN disk to calculate the electrolyte uptake.

The ionic conductivity evaluation was carried out with a symmetrical cell with SS electrodes, performing electrochemical impedance spectroscopy (EIS) measurements with a Biologic VSP potentiostat/galvanostat in the frequency range 100 kHz–100 mHz, with a perturbation amplitude of 5 mV around open circuit voltage (OCV) and recording 20 points per decade. The EIS spectra were acquired at 30 °C in a thermostatic oven.

A lithium iron phosphate (LFP) symmetrical cell was assembled for the galvanostatic charge/discharge test, for which a Biologic VSP potentiostat/galvanostat was used. The LFP electrode (LFP 60 E, NEI Corporation, composition: 88% active material, 8% binder, 4% conductive additive, mass loading = 13.7 mg cm^{-2}) was cut into disks of 9 mm in diameter and T-shaped BOLA cells were assembled.

Gel permeation chromatography (GPC) was carried out using a KNAUER system equipped with a refractive index detector and a TSKgel SuperHM-M column (length = 150 mm, internal diameter = 6 mm). Tetrahydrofuran (THF) was used as an eluant with a 0.6 mL min^{-1} flow and sample concentrations of about 5 mg mL^{-1}. The analyzed samples were solubilized in THF, stirred overnight, and filtered on a 0.45 μm PTFE filter. A molecular weight calibration curve was obtained with polystyrene standards in the molecular weight range 580–990500 g mol^{-1}.

Thermogravimetric analyses (TGA) were performed on a TA Instruments Q500 thermogravimetric analyzer. The analyses were conducted using the High-Resolution Dynamic mode with a sensitivity of 1, a maximum heating rate of 50 °C min^{-1} and a resolution number of 4, from ambient temperature to 700 °C under a nitrogen flow.

Differential scanning calorimetry (DSC) was carried out using a

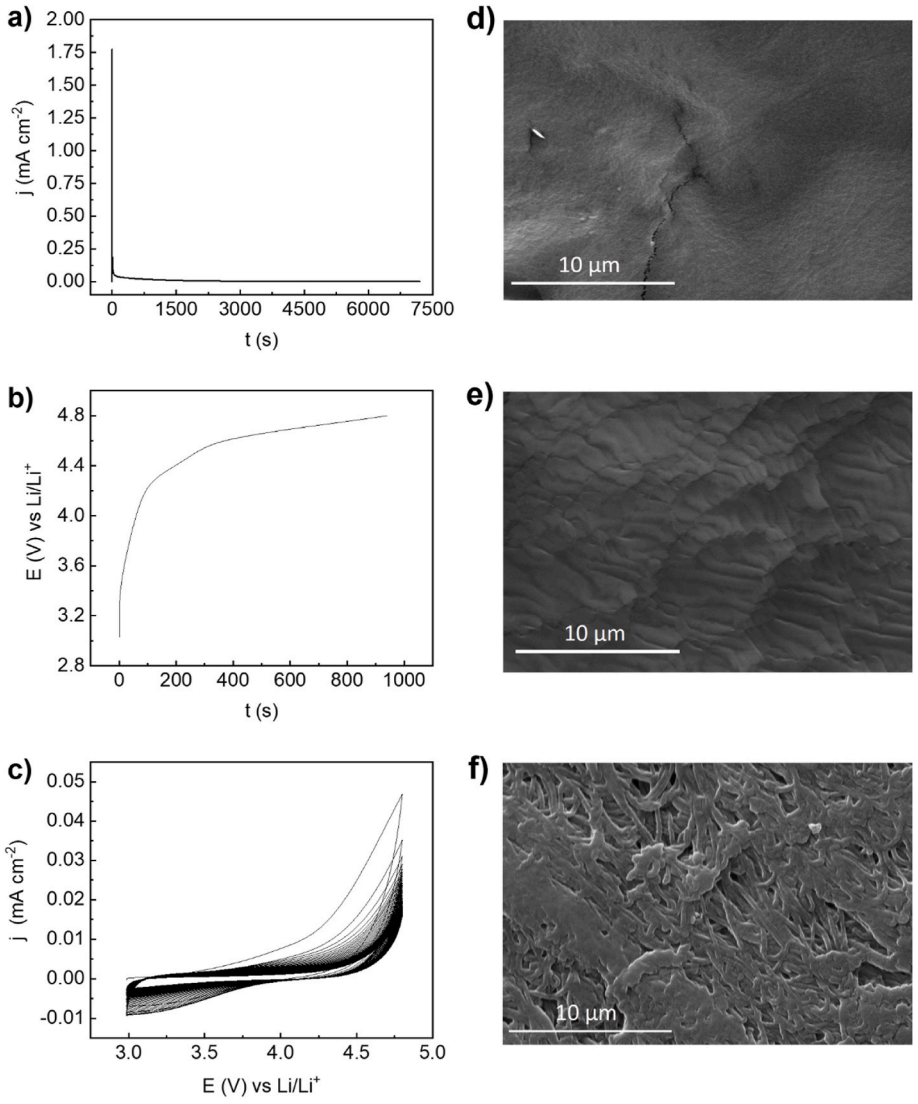

Fig. 1. Electro-initiated polymerization of DOL on PAN scaffold using different electrochemical techniques in Li//SS cell at 30 °C. CA at 4.8 V vs Li/Li^+ (a), CP at 25 µA (32 µA cm^{-2}) for 5 min (b), CV at 5 mV s^{-1} from OCV to 4.8 V vs Li/Li^+ for 100 cycles (c). SEM images of the PAN-PDOL electrolyte obtained by CA (d), CP (e), CV (f).

Q2000 DSC apparatus (TA instruments) equipped with a refrigerated cooling system (RCS90). The measurements were performed under nitrogen atmosphere in non-sealed aluminum pans. About 6 mg of PAN-PDOL sample underwent a heating scan at 20 °C min^{-1} from −90 °C to +130 °C, cooling at 10 °C min^{-1} to −90 °C, and then heated up again to 90 °C at 20 °C min^{-1}. A PAN-PDOL sample was also tested in a sealed pan, subjected to a heating scan at 5 °C min^{-1} from −90 °C to 90 °C, cooling at 10 °C min^{-1} to −90 °C, and then heated up again to 90 °C at 5 °C min^{-1}. From these acquired data, the glass transition temperature (T_g) was taken at half-height of the glass transition heat capacity step.

Temperature-modulated DSC (TMDSC) was performed from −90 to 200 °C on the PAN mat sample in non -sealed pan. The heating rate was 2 °C min^{-1}, the modulation amplitude was 0.8 °C and the oscillation period was 60 s. The T_g of PAN was determined from the reversing heat flow.

Dynamic mechanical thermal analysis (DMTA) was carried out on electrospun PAN strips and on PAN-PDOL electrolyte (gauge length about 10 mm) by means of a TA Instruments dynamic mechanical analyzer (DMA Q800), under tensile mode. The PAN-PDOL sample was tested within a heating ramp from −80 °C to 125 °C at 5 °C min^{-1}, adopting a frequency of 1 Hz under displacement control. The PAN sample was tested between −80 °C and 200 °C.

Scanning electron microscopy (SEM) was carried out on gold-coated samples with SEM Leica/Cambridge Stereoscan 360 operating at an accelerating voltage of 20 kV and software package INCA for morphological characterization.

Fourier-transform infrared spectroscopy FTIR spectra were collected by using a Bruker Alpha by accumulating a minimum of 64 scans per sample with a resolution of 2 cm^{-1} to inspect the PDOL formation.

^1H NMR spectra were recorded on a Bruker ADVANCE NEO 600 MHz spectrometer, equipped with liquid nitrogen chilled Bruker Prodigy (1H/19 F)-X broadband probe, using 30 s delay. The PAN-PDOL samples were immersed in THF-d_8 for 1 h before collecting the spectra.

3. Results and discussion

3.1. PAN-PDOL electrolyte preparation by DOL electro-initiated polymerization

The polymerization of DOL was first carried out in Li//SS cells by exploiting different electrochemical techniques: chronoamperometry (CA), chronopotentiometry (CP) and cyclic voltammetry (CV). The

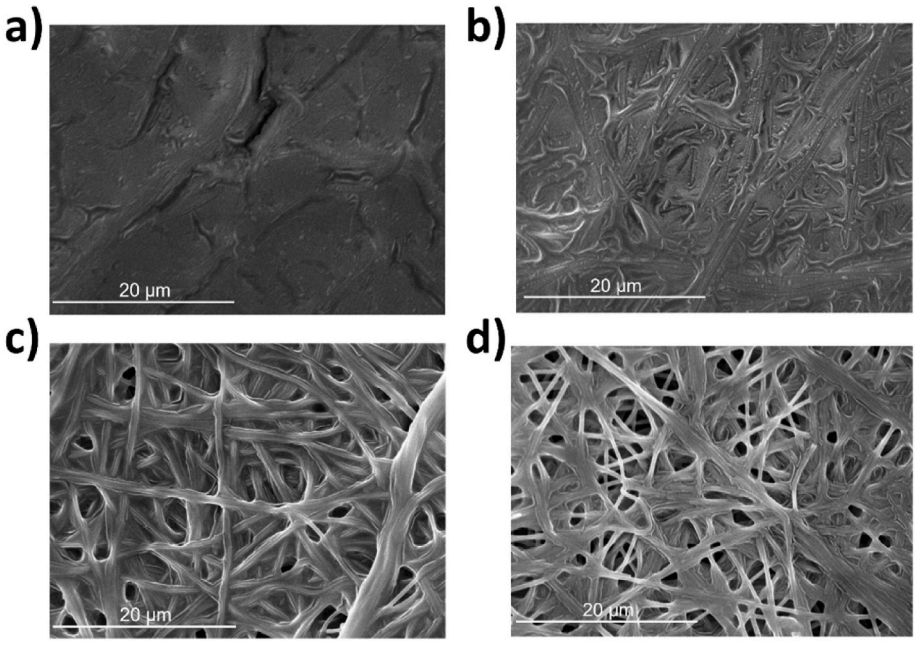

Fig. 2. SEM images of the in situ polymerized PDOL obtained in a symmetrical SS by CV at 5 mV s^{-1} from OCV to 2.9 V for 50 cycles using 100 μL (a), 30 μL (b), 10 μL (c) of 1.7 *m* LiTFSI-DOL solution, and 10 μL of 5 *m* LiTFSI-DOL solution (d).

LiTFSI-DOL solution was prepared with an O:Li ratio of 16:1, which resulted in a salt concentration of 1.7 m (mol kg^{-1}) and the electrospun PAN disk was imbibed with 100 μL of the solution. To have a clear indication of the potential, lithium metal has been used as both a counter and reference electrode. Even if the cell is cycled in two-electrode configuration, the relatively low current involved does not result in significant polarization of the lithium metal, which is used to get an indication of the potential range within which the polymerization takes place.

In the chronoamperometry test, a potential of 4.8 V vs Li/Li^+ was applied until the current reached a negligible value (Fig. 1a). For the chronopotentiometry technique, a current of 25 μA (32 μA cm^{-2}) was applied for 5 min, until it reached the cut-off potential of 4.8 V vs Li/Li^+ (Fig. 1b). PDOL was also obtained by cyclic voltammetry, going up to 4.8 V vs Li/Li^+ and back to OCV for several cycles (Fig. 1c).

SEM images of the in situ polymerized electrolyte showed the dependence of PDOL morphology from the electrochemical technique used for the polymerization. As a reference, the SEM image of the electrospun PAN mat is reported in Fig. S1. Imposing a constant potential or a constant current without rest, as in the case of CA (Fig. 1a and d) and CP (Fig. 1b and e), results in a rippled surface that completely masks the fibrous morphology of the PAN scaffold. Such kind of morphology results from a preferential polymerization at the electrode-electrolyte interface since the process proceeds at higher rates. Indeed, in CA the potential is forced to highly anodic potentials, while in CP the current imposed corresponds to the maximum current reached at ca. 5 V vs Li/Li^+ of the second cycle of the CV. In these cases, the uniform superficial layer of PDOL may act as a barrier for further oxidation and, hence, polymerization of the DOL monomer in the inner part of the PAN scaffold, with the possibility to have residual DOL inside the cell. In turn, the scarce formation of PDOL in the bulk of PAN membrane leads to an inhomogeneous PAN-PDOL solid electrolyte within the scaffold.

Instead, the sample prepared via cyclic voltammetry (Fig. 1c and f) displays the morphological features of the PAN fibers. In this case, the formation of the polymer is supposed to be more homogeneous along the whole sample. This is further confirmed by examining the oxidation charge during the electro-initiated polymerization. The charge recorded in CV is significantly higher (100 mC) compared to the lower values recorded in CA (32 mC) and in CP (23 mC). In CV, during the oxidation scan, DOL radicals are formed, initiating the polymerization process. Subsequently, during the reverse scan, the generation of radicals ceases, allowing the just formed radicals to polymerize into PDOL while the DOL monomers diffuse toward the electrode's surface to undergo oxidation in the subsequent cycle.

In contrast, with CA or CP, the formation of radicals persists throughout the entire duration of the applied current or potential. This sustained generation of radicals results in an uneven polymerization of PDOL within the PAN scaffold (Fig. 1d and e). Taking these considerations into account, cyclic voltammetry was selected as the preferred technique for the production of the electrolyte material.

The formation of the polymer electrolyte is confirmed in a SS/PAN-PDOL/SS by the increase in resistance observed in the Nyquist plot of the EIS analysis (Fig. S2a) in which, after the polymerization, the bulk resistance of the formed polymer electrolyte is visible in the high frequency part of the Nyquist plot. Moreover, FTIR analysis (Fig. S2b) shows the presence of peak related to the O–H stretching (ca. 3500 cm^{-1}), the intensity decrease of the DOL cyclic ether vibration at 925 cm^{-1}, and the changes of the *C*–O stretching (1100-1200 cm^{-1}) in the PDOL and PAN-PDOL spectra with respect to *C*–O of the DOL, which proves the formation of the polymer [24].

3.2. *Effect of LiTFSI-DOL solution amount and concentration*

To explore the effect of varying the volume of the LiTFSI-DOL solution employed in PDOL production, 100 μL, 30 μL and 10 μL of 1.7 *m* LiTFSI-DOL solution were added to the electrospun PAN scaffold. The PDOL was polymerized by CV in a symmetrical SS cell, more suitable for the conductivity tests than the Li/SS cell used before to evaluate the electrochemical potential window and the best technique for the in situ polymerization.

The formation and the morphology of the in situ polymerized PDOL has been assessed by SEM images. Fig. 2 shows the dependence of PDOL morphology from the amount of precursor used for the polymerization on the electrospun PAN mat. Decreasing the amount of precursor solution from 100 μL to 30 μL and 10 μL, makes the morphological features of the electrospun PAN more evident. Specifically, using 100 μL of precursor results in the formation of a continuous PDOL film that fully encapsulates the fibers and fills the pores entirely. Conversely, reducing

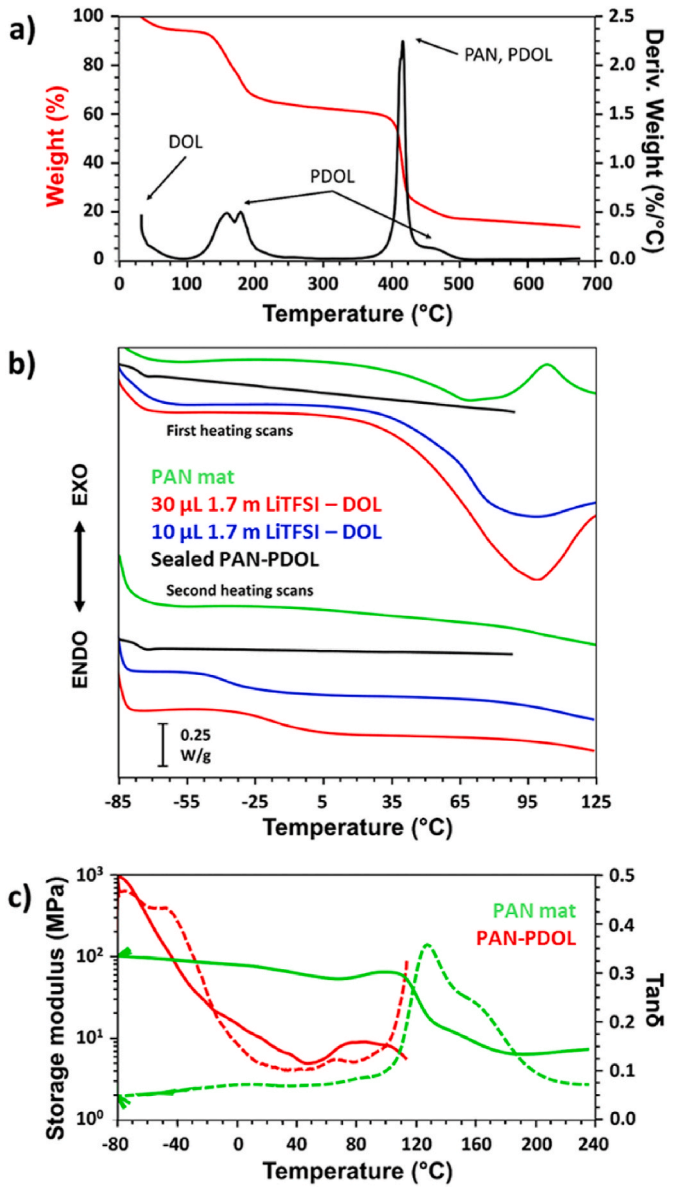

Fig. 3. TGA curve of PAN-PDOL sample obtained by CV electro-induced polymerization of 10 µL of 1.7 *m* LiTFSI-DOL solution in the PAN scaffold (a). DSC first and second heating scans of the PAN scaffold (green), PAN-PDOL with 30 µL (red) and 10 µL (blue) of 1.7 *m* LiTFSI-DOL solution in an open pan and PAN-PDOL 30 µL in sealed pan (black) (b). DMA of PAN scaffold (green) and PAN-PDOL with 30 µL of LiTFSI-DOL solution (red) showing the Storage Modulus (solid line) and Tanδ (dotted line) (c). (For interpretation of the references to colour in this figure legend, the reader is referred to the Web version of this article.)

the DOL to 30 µL leads to the formation of a polymeric film that does not completely occupy the pores of the electrospun scaffold. The in situ polymerized PDOL forms a thin coating on the surface of the PAN fibers when DOL amount is further reduced to 10 µL.

With the aim of decreasing the amount of free solvent inside the cell without decreasing too much the amount of salt, the concentration of the LiTFSI-DOL solution has been varied from 1.7 *m* to 5 *m*, which correspond to an O:Li ratio that ranges from 16:1 to 5:1. The morphology of the PAN-PDOL prepared with the more concentrated solution (Fig. 2d) is very similar to that reported in Fig. 2c.

The occurring of DOL polymerization, besides being confirmed by the formation of a solid material embedding the electrospun scaffold, is further confirmed by GPC analysis that demonstrates that the soluble fraction of the polymer contains molecular species with high molecular weights (Table S1). NMR further confirms the formation of the polymer and the presence of DOL residues (Fig. S3a). It is pointed out that, from these data it is not possible to evaluate the exact percentage of DOL and polymerized fraction because not all the polymer is solubilized. Indeed, SEM images of the PAN scaffold recovered after the immersion in THF d_8 (Fig. S3b) show that part of PDOL is still present on mats. This can also justify the high polydispersity resulting from GPC of the soluble fraction.

Fig. 3a shows the TGA analysis of the 10 µL sample that displays a first weight loss (about 5%) ascribable to liquid DOL present in the PAN sample which was not polymerized. As reported by Wang et al. [13], the second weight loss occurring in the range 100–200 °C is ascribed to the evaporation of DOL generated by the depolymerization of PDOL in presence of $TFSI^-$ anion. PAN degradation occurs at 400 °C, partially overlapped with PDOL degradation, and a last weight loss, attributed by Wang et al. [13] to PDOL degradation, is seen between 450 °C and 500 °C. The TGA of pure PDOL reported in Fig. S4 confirms this attribution. Therefore, TGA analysis confirms that the majority of the DOL imbibed in the PAN disk is polymerized, albeit a fraction is still in the monomer form, in line with NMR analysis (Fig. S3a). The formation of the PDOL is confirmed by the signals at 4.72 and 3.71 ppm, while the presence of DOL in the monomer form is evidenced by the peaks at 4.83 and 3.82 ppm. Quantitatively, the incomplete dissolution of PDOL in THF-d_8 (Fig. S3b) does not allow precise quantification of the DOL residue or of the PDOL degree of polymerization.

To further detect the presence of liquid DOL, DSC analysis was performed on PAN mat and PAN-PDOL samples (Fig. 3b). The DSC curve of PAN (Fig. 3b, green) is the overlay of different processes that make the interpretation non-trivial. TMDSC (Fig. S5) allowed to determine polymer T_g at 94 °C in the reversing heat flow curve, while the non-reversing heat flow curve showed an endothermal peak in the range 0–80 °C ascribable to water evaporation.

The DSC analysis of PAN-PDOL obtained with 10 µL (blue curve) and 30 µL (red curve) of the starting solution show a wide endothermal peak after 0 °C ascribable to the concomitant evaporation of water absorbed by PAN fibers and DOL residual monomer.

The enthalpy associated with this peak is higher in the sample prepared from 30 µL of solution ($\Delta H = 79.4\ J\ g^{-1}$) compared to the sample prepared with 10 µL of LiTFSI-DOL solution ($\Delta H = 40.6\ J\ g^{-1}$), being the amount of excess solution higher in the first case. In the second heating scan, the curves of PAN-PDOL samples only show the PDOL T_g at −40 °C after DOL loss, presumably not detectable in the first heating scan, due to the plasticizing effect of the monomer.

To further confirm this result, a PAN-PDOL sample was analyzed also in a sealed DSC pan (black curve). Under these conditions of analysis, no endothermal signals at high temperature are observed since the sample has achieved a vapor-liquid equilibrium within the sealed aluminum pan and the T_g of PDOL in the second heating scan was −80 °C due to the DOL plasticization effect.

Dynamic mechanical analysis (DMA) was performed both on the PAN mat and on the PAN-PDOL system obtained with 30 µL of the LiTFSI-DOL solution (Fig. 3c).

The initial storage modulus of PAN-PDOL sample at low temperatures is one order of magnitude higher than that of PAN fibers: this is due to the presence of pores in the PAN mat, which are filled with PDOL, strengthening the material. By increasing the temperature above the T_g of PDOL, the storage and loss modulus decrease as the material softens. The material is hardened at around 40 °C because of DOL evaporation and the loss of the plasticizing effect.

The DSC analysis (Fig. S6) confirms that, after the polymerization, in the case of 5 *m* concentration, less residual DOL is present in the PAN-PDOL sample, being the T_g of PDOL in the first heating scan equal to −61 °C, significantly higher than the T_g recorded at −80 °C in the samples prepared from 1.7 *m* solution. The ionic conductivity of the four samples was measured in symmetric SS//SS cells at 30 °C over time (Fig. 4a). The study of the conductivity has been performed only at 30 °C

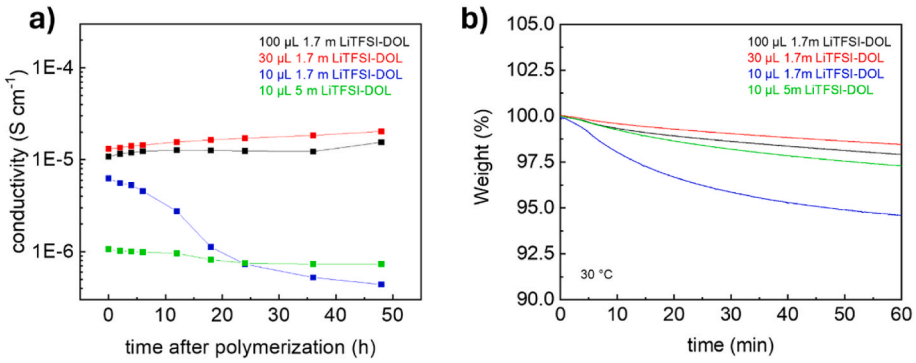

Fig. 4. Variation of the ionic conductivity at 30 °C over time (a) and isothermal TGA curves at 30 °C (b) of PAN-PDOL samples obtained with 100 µL (black), 30µL (red), 10 µL (blue) of 1.7 *m* LiTFSI-DOL starting solution, and 10 µL of 5 *m* LiTFSI-DOL solution (green). (For interpretation of the references to colour in this figure legend, the reader is referred to the Web version of this article.)

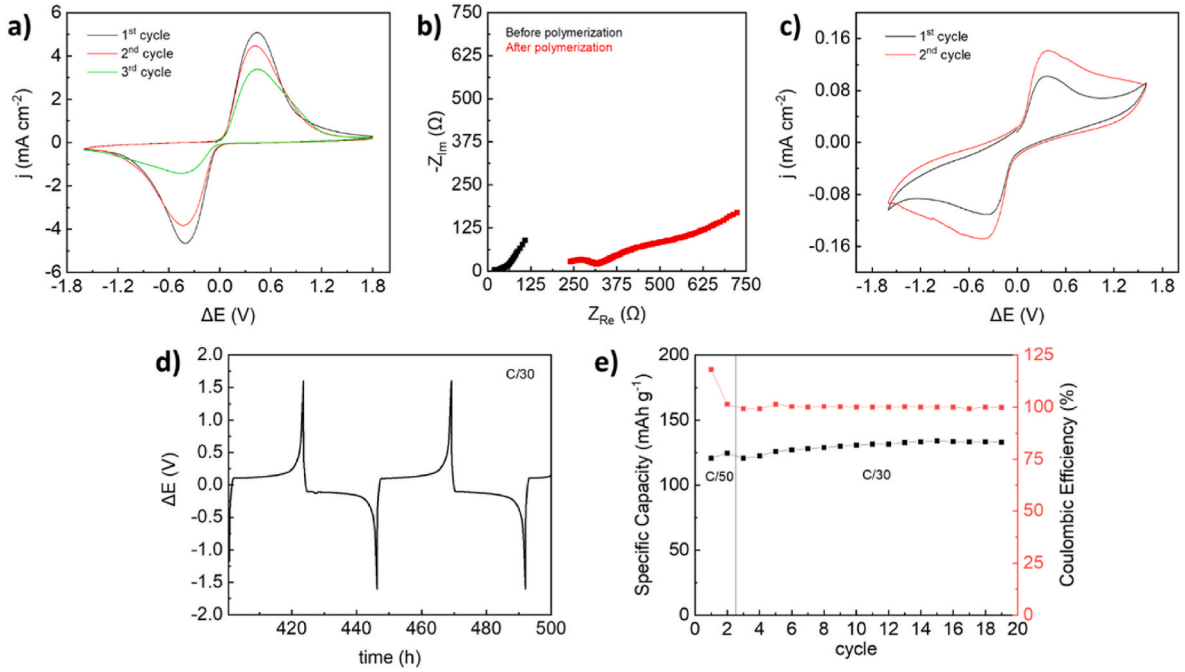

Fig. 5. Electrochemical measurements performed on the FP//LFP symmetrical cell. Cyclic voltammetry at 0.5 mV s^{-1} on the as assembled cell (a). EIS evolution before (black) and after (red) the in situ polymerization of DOL via CV (b). Cyclic voltammetry at 0.5 mV s^{-1} after the polymerization of DOL (c). Potential profile of two cycles at C/30 (j = 79 mA cm^{-2}) from the CD measurement with PAN-PDOL electrolyte (d). CD measurement specific capacity and coulombic efficiency with PAN-PDOL electrolyte (e). (For interpretation of the references to colour in this figure legend, the reader is referred to the Web version of this article.)

because DOL depletion during measurements at different temperatures does not allow proper comparison between the various systems, as evidenced by the isothermal TGA analysis (Fig. S7). The presence of DOL, which can act as a plasticizer for PDOL, boosts the ionic conductivity with respect to a real solid-state electrolyte. Indeed, the two samples with an excess of electrolyte (100 and 30 µL) exhibit a constant ionic conductivity higher than 10^{-5} S cm^{-1} over 2 days. Conversely, a different behavior affects the samples with the lowest amount of solution. In the case of the 10 µL 1.7 *m* LiTFSI-DOL sample, the conductivity decreases over time. It is worth noting that also in this case, the LiTFSI-DOL solution exceeds the scaffold volume uptake. However, the evaporation of the lower amount of residual DOL during the conductivity measurements leads to the transition from a gel-like electrolyte to a real solid state, and the reduction of the ionic conductivity from 6.3×10^{-5} S cm^{-1} to 4.4×10^{-7} S cm^{-1} is observed. The sample with the 5 *m* LiTFSI concentration displays a lower conductivity, as expected [31], but a lower decrease over time, probably due to the stronger interaction between salt and solvent. The isothermal TGA curves at 30 °C confirm this hypothesis, as shown in Fig. 4b.

3.3. Electrochemical test on PAN-PDOL electrolyte

The selection of FP//LFP cell for the evaluation of the polymer electrolyte stability has been mainly determined by the following reasons: it is the simplest symmetric cell and there is no Li metal that can affect the electrochemical response. Despite the lower conductivity, the electrolyte prepared with 10 µL of 5 *m* LiTFSI-DOL solution was used to assemble a symmetrical FP//LFP cell, in which the quasi solid-state electrolyte was polymerized in situ via CV. In the CV plot (Fig. 5a) the peaks related to Fe^{2+}/Fe^{3+} redox processes are clearly visible, while the process ascribed to the polymerization is not easily discernible (above 1.6 V, which is ca. 4.0 V vs Li/Li^{+}) due to the low current value involved in the DOL polymerization process. The decrease of the peak current density observed between the first and the third cycle can be ascribed to the lower ionic conductivity of the formed polymer electrolyte compared to the ionic conductivity of the 5 *m* LiTFSI-DOL solution. The

polymerization of the DOL was confirmed by the Nyquist plots (Fig. 5b), recorded just before polymerization and after a rest period of 24 h. After this period, two additional voltametric cycles were performed (Fig. 5c). The peak current density values decreased furtherly with respect to the third initial cycles of Fig. 5a, due to the electrolyte's polymerization over time.

Once the PDOL was formed, the charge-discharge cycles (CD) were carried out. The current density was kept relatively low as the low ionic conductivity of PAN-PDOL sample does not allow high current density to be applied because of the high ohmic drop. CD measurement with high mass loading electrodes (13.7 mg cm^{-2}) (Fig. 5d–e) shows that the symmetrical cell reaches a good specific capacity at C/30 of 134 mA h g^{-1}, which is 79% of the theoretical capacity of LFP. The higher coulombic efficiency of the first cycle is ascribed to a further polymerization process of liquid DOL still present in the cell. After the first cycles, the coulombic efficiency stabilizes around 100%. This result is particularly promising because in these conditions, with low current densities applied, the presence of undesired parasitic reactions would be accentuated. On the contrary, the high coulombic efficiencies achieved starting from the 3rd cycle indicate the electrolyte electrochemical stability with a relatively long calendar life (>950 h), where no further oxidation of DOL is occurring.

4. Conclusions

A solid-state polymer electrolyte obtained by in situ polymerization of 1,3-dioxolane was successfully prepared using different electrochemical techniques. The approach proposed intends to reduce the amount of a liquid phase and move closer to a real solid-state polymer electrolyte. The effect of the volume and concentration of the precursor solution used to prepare the poly (1,3-dioxolane) on a PAN scaffold was investigated and 10 μL of DOL is enough to produce the polymer electrolyte. If more DOL is used, the excess liquid phase boosts the ionic conductivity of the polymer electrolyte. Decreasing DOL amount and increasing the concentration of the salt made it possible to produce a PAN-PDOL polymer electrolyte with a minimized amount of residual DOL exhibiting good compatibility with the cathodic material proposed, with a relatively long calendar life (>950 h), as assessed by a FP//LFP cell, with LFP specific capacity of 134 mA h g^{-1}. Further studies on the viability of the presented electrolyte with lithium metal anodes can be addressed by introducing additives for the lithium metal protection.

CRediT authorship contribution statement

Nicolò Albanelli: Data curation, Formal analysis, Investigation, Visualization, Writing – original draft, Writing – review & editing. **Francesco Capodarca:** Data curation, Investigation. **Michele Zanoni:** Data curation, Formal analysis, Investigation, Visualization, Writing – original draft, Writing – review & editing. **Giampaolo Lacarbonara:** Data curation, Formal analysis, Visualization, Writing – review & editing. **Maria Letizia Focarete:** Methodology, Resources, Writing – review & editing. **Chiara Gualandi:** Methodology, Resources, Writing – review & editing. **Catia Arbizzani:** Conceptualization, Methodology, Resources, Supervision, Writing – original draft, Writing – review & editing.

Declaration of competing interest

The authors declare that they have no known competing financial interests or personal relationships that could have appeared to influence the work reported in this paper.

Data availability

Data will be made available on request.

Acknowledgements

Work funded by the Italian MUR (PNRR funds-CNMS-Spoke 13-MOST Code: CN00000023).

Appendix A. Supplementary data

Supplementary data to this article can be found online at https://doi.org/10.1016/j.powera.2024.100140.

References

[1] Y. Chen, Y. Kang, Y. Zhao, L. Wang, J. Liu, Y. Li, Z. Liang, X. He, X. Li, N. Tavajohi, B. Li, A review of lithium-ion battery safety concerns: the issues, strategies, and testing standards, J. Energy Chem. 59 (2021) 83–99, https://doi.org/10.1016/j.jechem.2020.10.017.

[2] C. Li, Z. Wang, Z. He, Y. Li, J. Mao, K. Dai, C. Yan, J. Zheng, An advance review of solid-state battery: challenges, progress and prospects, Sustainable Materials and Technology 29 (2021) e00297, https://doi.org/10.1016/j.susmat.2021.e00297.

[3] Z. Xue, D. He, X. Xie, Poly(ethylene oxide)-based electrolytes for lithium ion batteries, J. Mater. Chem. A 3 (2015) 19218–19253, https://doi.org/10.1039/C5TA03471J.

[4] Z. Song, F. Chen, M. Martinez-Ibañez, W. Feng, M. Forsyth, Z. Zhou, M. Armand, H. Zhang, A reflection on polymer electrolytes for solid-state lithium metal batteries, Nat. Commun. 14 (2023) 4884, https://doi.org/10.1038/41467-023-40609-y.

[5] S. Xia, X. Wu, Z. Zhang, Y. Cui, W. Liu, Practical challenges and future perspectives of all-solid-state lithium-metal batteries, Chem 5 (2019) 753–785, https://doi.org/10.1016/j.chempr.2018.11.013.

[6] D. Aurbach, O. Youngman, Y. Gofer, A. Meitav, P. Dan, The electrochemical behaviour of 1,3-dioxolane—LiClO4 solutions—I. Uncontaminated solutions, Electrochim, Acta 35 (1990) 625–638, https://doi.org/10.1016/0013-4686(90)87055-7.

[7] D. Aurbach, O. Youngman, P. Dan, The electrochemical behavior of 1,3-dioxolane—$LiClO_4$ solutions—II. Contaminated solutions, Electrochim. Acta 35 (1990) 639–655, https://doi.org/10.1016/0013-4686(90)87056-8.

[8] H. Zhong, Z. Xu, F. Ding, A novel quasi-solid state electrolyte with highly effective polysulfide diffusion inhibition for lithium-sulfur batteries, Sci. Rep. 6 (2016) 25484, https://doi.org/10.1038/srep25484.

[9] G. Xu, A. Kushima, J. Yuan, H. Dou, W. Xue, X. Zhang, X. Yan, J. Li, Ad hoc solid electrolyte on acidized carbon nanotube paper improves cycle life of lithium–sulfur batteries, Energy Environ. Sci. 10 (2017) 2544–2551, https://doi.org/10.1039/C7EE01898C.

[10] A. La Monaca, F. De Giorgio, F. Soavi, G. Tarquini, M. Di Carli, P.P. Prosini, C. Arbizzani, 1,3-Dioxolane: a strategy to improve electrode interfaces in lithium ion and lithium-sulfur batteries, Chemelectrochem 5 (2018) 1272–1278, https://doi.org/10.1002/celc.201701348.

[11] C. Qu, Y. Chen, X. Yang, H. Zhang, X. Lia, H. Zhang, LiNO3-free electrolyte for Li-S battery: a solvent of choice with low Ksp of polysulfide and low dendrite of lithium, Nano Energy 39 (2017) 262–272, https://doi.org/10.1016/j.nanoen.2017.07.002.

[12] L. Kong, H. Zhan, Y. Li, Y. Zhou, In situ fabrication of lithium polymer battery basing on a novel electropolymerization technique, Electrochem. Commun. 9 (2007) 2557–2563, https://doi.org/10.1016/j.elecom.2007.08.001.

[13] Y. Wang, R. Xu, B. Xiao, D. Lv, Y. Peng, Y. Zheng, Y. Shen, J. Chai, X. Lei, S. Luo, X. Wang, X. Liang, J. Feng, Z. Liu, A poly(1,3-dioxolane) based deep-eutectic polymer electrolyte for high performance ambient polymer lithium battery, Mater. Today Phys. 22 (2022) 100620, https://doi.org/10.1016/j.mtphys.2022.100620.

[14] H. Li, Y. Du, L. Zhao, C. Xiong, E. Zhao, C. Li, S. Hao, W. Zhou, Traditional poly (1,3-dioxolane) electrolytes via integrated design of ultra-stable network for solid-state lithium metal batteries, Res Sq, PREPRINT. DOI: 10.21203/rs.3.rs-2003311/v1.

[15] Z. Wang, Y. Wang, L. Shen, Z. Jin, H.M. Law, A. Wang, W. Wang, F. Ciucci, Towards durable practical lithium–metal batteries: advancing the feasibility of poly-DOL-based quasi-solid-state electrolytes via a novel nitrate based additive, Energy Environ. Sci. 16 (2023) 4084, https://doi.org/10.1039/d3ee02020g.

[16] G. Yang, Y. Zhai, J. Yao, S. Song, L. Lin, W. Tang, Z. Wen, N. Hu, L. Lu, Synthesis and properties of poly(1,3-dioxolane) in situ quasi-solid-state electrolytes via a rare earth triflate catalyst, Chem. Commun. 57 (2021) 7934, https://doi.org/10.1039/d1cc02916a.

[17] J. Yu, X. Lin, J. Liu, J.T.T. Yu, M.J. Robson, G. Zhou, H.M. Law, H. Wang, B. Z. Tang, F. Ciucci, In situ fabricated quasi-solid polymer electrolyte for high-energy-density lithium metal battery capable of subzero operation, Adv. Energy Mater. 12 (2022) 2102932, https://doi.org/10.1002/aenm.202102932.

[18] B. Deng, M.-X. Jing, R. Li, L.-X. Li, H. Yang, M.-Q. Liu, J. Xiang, W.-Y. Yuan, X.-Q. Shen, Integrating high ionic conductive PDOL solid/gel composite electrolyte for enhancement of interface combination and lithium dentrite inhibition of solid-state lithium battery, J. Colloid Interface Sci. 620 (2022) 199–208, https://doi.org/10.1016/j.jcis.2022.04.008.

[19] Z.-H. Huang, M.-X. Jing, P.-Q. Wang, W.-W. Shao, Z.-P. Zhang, G. Zhang, X.-Q. Shen, A high ionic conductive PDOL/LAGP composite solid electrolyte film for Interfacial Stable solid-state lithium batteries, Ceram. Int. 49 (2023) 5510–5517, https://doi.org/10.1016/j.ceramint.2022.10.074.

[20] L.-X. Li, R. Li, Z.-H. Huang, H. Yang, M.-Q. Liu, J. Xiang, S. Hussain, X.-Q. Shen, M.-X. Jing, A multifunctional gradient solid electrolyte remarkably improving interface compatibility and ion transport in solid-state lithium battery, ACS Appl. Mater. Interfaces 14 (2022) 30786–30795, https://doi.org/10.1021/acsami.2c05578.

[21] H. Yang, B. Zhang, M. Jing, X. Shen, L. Wang, H. Xu, X. Yan, X. He, In situ catalytic polymerization of a highly homogeneous PDOL composite electrolyte for long-cycle high-voltage solid-state lithium batteries, Adv. Energy Mater. 12 (2022) 2201762, https://doi.org/10.1002/aenm.202201762.

[22] J. Cui, Y. Du, L. Zhao, X. Li, Z. Sun, D. Li, H. Li, Thermal stable poly-dioxolane based electrolytes via a robust crosslinked network for dendrite-free solid-state li-metal batteries, Chem. Eng. J. 461 (2023) 141973, https://doi.org/10.1016/j.cej.2023.141973.

[23] Y. Bai, W. Ma, W. Dong, Y. Wu, X. Wang, F. Huang, In-situ-polymerized 1,3-dioxolane solid-state electrolyte with space-confined plasticizers for high-voltage and robust Li/$LiCoO_2$ batteries, ACS Appl. Mater. Interfaces 15 (2023) 26834–26842, https://doi.org/10.1021/acsami.3c04234.

[24] D. Chen, M. Zhu, P. Kang, T. Zhu, H. Yuan, J. Lan, X. Yang, G. Sui, Self-enhancing gel polymer electrolyte by in situ construction for enabling safe lithium metal battery, Adv. Sci. 9 (2022) 2103663, https://doi.org/10.1002/advs.202103663.

[25] Y. Liu, Y. Xu, Porous membrane host-derived in-situ polymer electrolytes with double-stabilized electrode interface enable long cycling lithium metal batteries, Chem. Eng. J. 433 (2022) 134471, https://doi.org/10.1016/j.cej.2021.134471.

[26] C. Liu, R.L. Sacci, R. Sahore, G.M. Veith, N.J. Dudney, X.C. Chen, Polyacrylonitrile-based electrolytes: how processing and residual solvent affect ion transport and stability, J. Power Sources 527 (2022) 231165, https://doi.org/10.1016/j.jpowsour.2022.231165.

[27] X. Yu, M. Li, L. wei, J. Qiu, G. Cao, Y. Wen, Application of polyacrylonitrile in the electrolytes of lithium metal batteries, Prog. Chem. 35 (3) (2023) 390–406, https://doi.org/10.7536/PC220913.

[28] F. Croce, F. Gerace, G. Dautzemberg, S. Passerini, G.B. Appetecchi, B. Scrosati, Synthesis and characterization of highly conducting gel electrolytes, Electrochim. Acta 39 (14) (1994) 2187–2194.

[29] P. Shi, Z.-Y. Liu, X.-Q. Zhang, X. Chen, N. Yao, J. Xie, C.-B. Jin, Y.-X. Zhan, G. Ye, J.-Q. Huang, S. Ifan, M.-M. Titirici, Q. Zhang, Polar interaction of polymer host–solvent enables stable solid electrolyte interphase in composite lithium metal anodes, J. Energy Chem. 64 (2022) 172–178, https://doi.org/10.1016/j.jechem.2021.04.045.

[30] H. Gao, N.S. Grundish, Y. Zhao, A. Zhou, J.B. Goodenough, Formation of stable interphase of polymer-in-salt electrolyte in all-solid-state lithium batteries, Energy Material Advances (2021) 1932952, https://doi.org/10.34133/2021/1932952.

[31] R. Raccichini, J.W. Dibden, A. Brew, J.R. Owen, N. García-Aráez, Ion speciation and transport properties of LiTFSI in 1,3-dioxolane solutions: a case study for Li−S battery applications, J. Phys. Chem. B 122 (2018) 267–274, https://doi.org/10.1021/acs.jpcb.7b09614.